Title
Protein footprinting by pyrite shrink-wrap laminate

Journal
Lab on a Chip, 15(7)

ISSN
1473-0197

Authors
Leser, Micheal
Pegan, Jonathan
Makkaoui, Mohammed El
et al.

Publication Date
2015-04-07

DOI
10.1039/c4lc01288g

Peer reviewed

Published in final edited form as:

Lab Chip. 2015 April 07; 15(7): 1646–1650. doi:10.1039/c4lc01288g.

Protein Footprinting by Pyrite Shrink-Wrap Laminate

Micheal Leser[1,§], **Jonathan Pegan**[2,§], **Mohammed El Makkaoui**[3,4,§], **Joerg C. Schlatterer**[1,¶], **Michelle Khine**[2,4,*], **Matt Law**[3,4,*], **Michael Brenowitz**[1,*]

[1]Department of Biochemistry, Albert Einstein College of Medicine, Bronx, NY

[2]Department of Biomedical Engineering, University of California, Irvine, CA

[3]Department of Chemistry, University of California, Irvine, CA

[4]Department of Chemical Engineering & Materials Science, University of California, Irvine, CA

Abstract

The structure of macromolecules and their complexes dictate their biological function. In "footprinting", the solvent accessibility of the residues that constitute proteins, DNA and RNA can be determined from their reactivity to an exogenous reagent such as the hydroxyl radical (•OH). While •OH generation for protein footprinting is achieved by radiolysis, photolysis and electrochemistry, we present a simpler solution. A thin film of pyrite (cubic FeS_2) nanocrystals deposited onto a shape memory polymer (commodity shrink-wrap film) generates sufficient •OH via Fenton chemistry for oxidative footprinting analysis of proteins. We demonstrate that varying either time or H_2O_2 concentration yields the required •OH dose–oxidation response relationship. A simple and scalable sample handling protocol is enabled by thermoforming the "pyrite shrink-wrap laminate" into a standard microtiter plate format. The low-cost and malleability of the laminate facilitates its integration into high throughput screening and microfluidic devices.

Introduction

In "footprinting", the solvent accessibility of individual residues of biological macromolecules is measured by their reactivity to an exogenous reagent.[1, 2] The hydroxyl radical (•OH) is an effective footprinting probe due to its high reactivity and small size.[3] Nucleic acid •OH footprinting monitors backbone polysaccharide cleavage.[4] Mapping of DNA structure and protein binding[4] was followed by study of RNA structure and folding.[5] Quantification of side chain oxidation is the dominant mode of protein footprinting analyses.[2] Footprinting isotherms and time progress curves linked to local structural transitions resolve macromolecular binding and folding mechanisms.[6]

*Correspondence may be addressed to mkhine@uci.edu, matt.law@uci.edu & michael.brenowitz@einstein.yu.edu.
§These authors contributed equally to this study
¶Present address: Division of Graduate Education, Directorate for Education and Human Resources, National Science Foundation (NSF), 4201 Wilson Boulevard, Arlington, VA 22230, USA. Any opinion, finding, conclusions, or recommendations expressed in this material are those of the author and do not necessarily reflect the views of the NSF.

Electronic Supplementary Information (ESI) available: [details of any supplementary information available should be included here]. See DOI: 10.1039/b000000x/

Ascorbate-driven Fenton chemistry mediated by $[Fe(edta)]^{2-}$ is widely used for nucleic acid •OH footprinting.[4] The coupled reactions are $Fe^{2+} + H_2O_2 \rightarrow Fe^{3+} + HO\bullet + OH^-$ (1) and $Fe^{3+} + H_2O_2 \rightarrow Fe^{2+} + HOO\bullet + H^+$ (2). Ascorbate facilitates •OH generation by reducing the Fe^{3+}. Variations include using reaction 1 alone to study fast structural transitions,[7] or dissolved O_2 instead of H_2O_2,[8] and substituting peroxonitrous acid for $[Fe(edta)]2^-$ and H_2O_2.[9]. Radiolysis of water by low flux gamma[10] and high flux synchrotron radiation,[11, 12] pulsed electron beam,[13] laser photolysis of H_2O_2[14] and electrochemical oxidation[15] are used to generate •OH for protein footprinting. The latter approaches require specialized equipment for radical generation, fluid flow management and sample collection.

The mineral iron pyrite (cubic FeS_2) supports Fenton chemistry. [16] Powdered pyrite in a microfluidic device footprints DNA and RNA.[17, 18] However, powdered mineral proved incompatible with multiplexed microfluidic mixers due to slow and uneven flow rates (Jones, CD, Schlatterer, JC, Brenowitz, M & Pollack L; unpublished). Herein we describe the deposition of pyrite nanocrystal films[19] onto shape memory polymer (commodity shrink-wrap film[20]) to create a novel mediator of Fenton chemistry. Thermally inducing the pyrite-coated shrink film to retract causes the stiffer nanocrystalline layer to buckle, resulting in a highly reactive, wrinkled and robustly integrated laminate of pyrite nanocrystals. Sample wells thermoformed into the laminate in a standard well format enables footprinting to be carried out by the simple deposition and removal of sample drops. We demonstrate the utility of pyrite shrink-warp laminate for the controlled generation of •OH for oxidative protein footprinting.

Materials and Methods

The pyrite nanocrystals are prepared via a hot-injection method based on the synthesis of Puthussery *et al.*[19] as detailed in the Supplement. The pyrite colloidal suspension is spray coated onto 4” × 4” shape-memory polyolefin sheets (Cryovac D955, Sealed Air) using a handheld Badger Model 200 airbrush (Fig. 1A; Supplemental Video). Polyolefin sheets are pinned to PMMA substrates and mounted vertically in a fume hood. Spray coating is performed twice at room temperature with manual sweeps of ~ 3 s from a distance of 8 inches descending from top to bottom; 5 mL of suspension are consumed for each coat. Ligand exchange is not performed.

The coated polyolefin sheets are quickly shrunk by 95% at 160 °C by waving a heat gun (HL 1810 S, Steinel) above its surface (Figs. 1A & 1B; [21]). Binder clips attached to the corners prevent the sheets from crumpling. Microwells are thermoformed into the shrunk laminate (Figs. 1C & D) using a 384 well template patterned into CO_2 laser cut (Versalaser) 3 mm thick PMMA (McMaster-Carr) The laminate is held on top of the template with a vacuum and then gently heated above the glass transition temperature of the polyolefin (125 °C) with the heat gun. The pressure difference pushes the laminate into the template vias to form the microwells (Fig. 1D).

A 16 well pyrite shrink laminate chip (Fig. 1C) is affixed to a tabletop-mounted vibration motor (10,000 RPM, (Amico UPC 610-696811493, Amazon.com). Surface oxidation is removed by adding 5 μL of 0.1 M HCl to the microwells for 5 min followed by several

water washes to neutralize the acid (Fig. 3). Measurement of the fluorescence loss of an aromatic dye is a convenient way to assess relative rates of •OH production as described in the Supplement.

In our protein studies, aliquots of recombinant BirA-tagged mouse Programmed Death 1 (PD-1) are dialyzed into standard reaction buffer (20 mM sodium cacodylate pH 8.0, 50 mM NaCl, 1 mM EDTA) and diluted to 100 μM just prior to oxidation.

Fig. 2 summarizes 'drop deposition oxidation'. Just prior to initiating oxidation, 0.6 and 2.4 μL of stock solutions of sodium ascorbate and H_2O_2, respectively are added to 27 μL of protein or dye in buffer to the desired concentrations. A 3 μL aliquot is pipetted into a pyrite shrink-wrap laminate microwell and vibration is started to mix the sample. Following incubation (1 min unless noted), the vibration is terminated and the sample transferred by pipet to 27 μL of a 'quench solution' containing 34 μM thiourea, 12 μM methioninamide and 13 μg/mL catalase[22]. Protein samples are snap frozen on dry ice and stored at −20 °C for analysis by mass spectrometry.

Standard protocols described in the Supplement are used to prepare PD-1 for analysis by MALDI-TOF mass spectroscopy. PD-1 is digested with trypsin and MALDI-TOF spectra from 800-5000 m/z are collected and normalized against the total peptide present in a sample. Protein Prospector (UCSF) is used to predict the peptide masses of the MALDI precursor ions. Peaks corresponding to unmodified and oxidized (+16, +32, +48, etc.) states of each peptide are visually identified. The fraction of unmodified peptide is calculated from the ratio of the normalized intensity of the unmodified peptide peaks to the sum of the intensities of both the unmodified and oxidized peaks of that peptide. Plotting the fraction of unmodified peptide against oxidation time or H_2O_2 concentration yields dose-response curves that are fit by non-linear regression in GraphPad Prism 6.

Results

Pyrite nanocrystal colloidal suspension is easily sprayed on shape-memory polyolefin using an art supply airbrush (Fig. 1A; Supplemental Video). A single pass deposits a 50 ± 25 nm coating (Fig. 3C). Two coats are applied. The sprayed layers are phase-pure pyrite as assayed by powder X-ray diffraction and Raman spectroscopy (data not shown). The ~95% area reduction of shrunk shape-memory polyolefin results in 20 fold compression of the planar surface area (Fig. 1B). Top-down SEMs show wrinkling of the pyrite coating (Fig. 3A & B) similar to metal thin films.[23] Cyclic voltammetry of gold films shows > 600% increased surface area. Similar enhancement is expected for pyrite laminate due to the similar surface topology.[24]

Thermoforming microwells into shrink-wrap laminate is straightforward. We patterned wells in the 384 well format drawn to a depth sufficient to hold 3 μL (Figs. 1C & D). The wells enable a simple sample handling protocol that we call 'drop deposition' to be implemented with standard single or multi-channel pipettes. Microfluidics are not required.

Pyrite shrink-wrap laminate has properties that facilitate its use. The pyrite nanocrystalline coating integrates with the plastic during shrinkage, resulting in a hard, robust laminate.

A ‘tape test’ performed on several laminate samples showed no visible transfer of pyrite from the laminate to the tape, demonstrating good mechanical integration of the pyrite nanocrystal film to the polyolefin (data not shown). Pyrite shrink-wrap laminate maintains its •OH generation efficiency for at least 14 months during storage in ambient conditions (Supplementary Fig. 1).

Optimization of •OH generation as a function of either time or H_2O_2 concentration was accomplished by quantifying the oxidation of the dye fluorescein. Loss of dye fluorescence is proportional to •OH concentration. In our protocol, 3 μL drops of sample solution are deposited, incubated and removed from the microwells (Fig. 2). The robust radical production evident on pyrite shrink-wrap laminate is enhanced by vibration during sample incubation, presumably by maximizing interaction of the solution with the pyrite surface (Fig. 3D). The comparison of natural pyrite mineral, pyrite nanocrystals deposited on silicon, and pyrite shrink-wrap laminate shows that both the nanocrystalline form of pyrite and the laminate’s wrinkled surface topology contribute to •OH production (Fig. 4B).

The production of •OH from pyrite shrink-wrap laminate was optimized by systematically varying the concentrations of sodium ascorbate and H_2O_2. Excessive ascorbate reduces the •OH available to oxidize substrates since it is also a radical scavenger.[25] Ascorbate at 1 mM maximizes •OH production for H_2O_2 concentrations from 0 to 2 mM (Fig. 4A). We observe the exponential decay characteristic of a Poisson distribution with pyrite-shrink-wrap laminate when •OH production is controlled by either H_2O_2 concentration or incubation time (Fig. 4C). Achieving ‘single-hit’ distribution of modification or cleavage events is essential to quantitative footprinting[2, 26] and is conveniently achieved in our standard protocol by varying the H_2O_2 concentration at a constant time of 1 min.

To determine whether pyrite shrink-wrap laminate facilitates •OH generation by reaction on its surface or through iron dissolved from the surface, we measured the release of ferrous iron to determine during our standard reaction conditions. Only ~1.5 μM of iron is leached during our standard 1 min of oxidation independent of H_2O_2 concentration (Supplementary Fig. 2). To put this amount of solution iron in perspective, we compared •OH production from the laminate with that from 2 μM $[Fe(edta)]2^-$ at common H_2O_2 and ascorbate concentrations and incubation time (Fig. 5). That the laminate produces greater •OH mediated oxidation suggests that the surface is the dominant source of •OH from pyrite shrink-wrap laminate.

The PD-1 protein retains its native fold following exposure to either shrink plastic or pyrite shrink-wrap laminate (Supplemental Fig. 3). PD-1 samples were incubated on pyrite-shrink-wrap laminate following our standard protocol as a function of H_2O_2 concentration and analyzed by MALDI (Fig. 3 & Supplement). MALDI is suitable for this study due to the protein’s small size; peptides containing >90% of its sequence are detectable (data not shown). The N-terminal peptide (1-36) of PD-1 contains four residues susceptible to oxidation and accessible by solvent – Y4, W8, W26, and M31 (Fig. 6B, insert). The +16 ions and multiples thereof are evident as the •OH dose increases as a function of increasing H_2O_2 concentration (Fig. 6A). Peptide oxidation is described by an exponential decay consistent with the Poisson distribution (Fig. 6B). Oxidation was extended well

beyond ‘single-hit’ in this figure to demonstrate the efficacy of •OH generation (Fig. 6A); a footprinting analysis would use lower the H_2O_2 concentrations to determine solvent accessibility and LC-MS/MS to isolate the oxidation of each of the susceptible residues.

Discussion

With the advent of protein therapeutics, there is an increased need to develop facile high-throughput methods to determine protein structure in support of product development, validation and regulatory approval. While atomic resolution models of macromolecular complexes are the gold standard for structure, oxidative footprinting can contribute to the therapeutic development pipeline by rapidly and inexpensively mapping the molecular interfaces that mediate a biological activity. Our goal in creating pyrite shrink-wrap laminate is to lower the barrier to oxidative protein footprinting by eliminating the need for a source of ionizing radiation, a UV laser and/or microfluidic sample handling. The sole requirement is a standard laboratory pipette; higher throughput can be achieved with a multi-channel pipette or robotic sample handler. Pyrite can also be used to study nucleic acids and their complexes with proteins.[17, 18]

Pyrite shrink-wrap laminate is inexpensive to fabricate. While the synthesis of pyrite nanocrystals requires expertise and an appropriately equipped laboratory, it is a straightforward and scalable process. Similarly scalable is the airbrush deposition of pyrite nanocrystals. We have prepared prototype shrink-wrap pieces the size of a standard microtiter plate, demonstrating a clear path to scaling up to support robotic sample handling systems (data not shown). The ability to store pyrite shrink-wrap laminate for over a year in ambient conditions will facilitate its dissemination and adoption.

The laminate is a promising material for the development of other active surfaces and microfluidic reactors due to bonding of the deposited material to the plastic and the enhanced surface area that results from shrinkage. Microwell fabrication is completely flexible. The number and volume of the wells is tailored by configuration of the PMMA template. Indeed, troughs, serpentine and branched patterns could be molded in the laminate for use in microfluidic applications. Other materials could be deposited that would facilitate or catalyze other chemical reactions. Thus, shrink-wrap laminate is a versatile platform with regard to both rapid physical configuration and chemical functionality for the development of novel applications.

Key to the effectiveness of pyrite shrink-wrap laminate is that •OH dose can be precisely controlled, allowing protein side chain oxidation rates to be calculated. This characteristic, together with a scalable and customizable form factor, facilitates integration with microfluidics and higher-throughput analysis without the need for infrastructure. We are applying this approach to the analysis of immunological recognition complexes. The next challenge to address is the integration of multiple structural maps into robust models of molecular structure to be applied to scientific discovery and industrial processing.

Supplementary Material

Refer to Web version on PubMed Central for supplementary material.

Acknowledgements

This project was supported by NSF-IDBR 0852796 (M.B), the Biomolecular Interaction Technologies Center, a NSF Industry / University Cooperative Research Center (M.B), NIH DP2 OD007283-01 (M.K.) and the U.S. DOE DE-EE0005324, funded by the SunShot Next Generation Photovoltaics II (NextGen PVII) program (M.L. and M.E.M.). We thank Steve Almo and his colleagues for providing PD-1 protein, and Edward Nieves and Jennifer Aguilan for assistance with mass spectrometry.

Notes and references

1. Petri V and Brenowitz M, Current opinion in biotechnology, 1997, 8, 36–44. [PubMed: 9013649]
2. Takamoto K and Chance MR, Annual review of biophysics and biomolecular structure, 2006, 35, 251–276.
3. Buxton GV, Greenstock CL, Helman WP and Ross AB, J Phys Chem Ref Data, 1988, 17, 513–886.
4. Tullius TD and Dombroski BA, Proceedings of the National Academy of Sciences of the United States of America, 1986, 83, 5469–5473. [PubMed: 3090544]
5. Sclavi B, Sullivan M, Chance MR, Brenowitz M and Woodson SA, Science, 1998, 279, 1940–1943. [PubMed: 9506944]
6. Brenowitz M, Chance MR, Dhavan G and Takamoto K, Current opinion in structural biology, 2002, 12, 648–653. [PubMed: 12464318]
7. Shcherbakova I, Mitra S, Beer RH and Brenowitz M, Nucleic acids research, 2006, 34, e48. [PubMed: 16582097]
8. Takamoto K, Das R, He Q, Doniach S, Brenowitz M, Herschlag D and Chance MR, Journal of molecular biology, 2004, 343, 1195–1206. [PubMed: 15491606]
9. King PA, Jamison E, Strahs D, Anderson VE and Brenowitz M, Nucleic acids research, 1993, 21, 2473–2478. [PubMed: 8389444]
10. Hayes JJ, Kam L and Tullius TD, Methods in enzymology, 1990, 186, 545–549. [PubMed: 2172714]
11. Sclavi B, Woodson S, Sullivan M, Chance MR and Brenowitz M, Journal of molecular biology, 1997, 266, 144–159. [PubMed: 9054977]
12. Maleknia SD, Brenowitz M and Chance MR, Analytical chemistry, 1999, 71, 3965–3973. [PubMed: 10500483]
13. Watson C, Janik I, Zhuang T, Charvatova O, Woods RJ and Sharp JS, Analytical chemistry, 2009, 81, 2496–2505. [PubMed: 19265387]
14. Hambly DM and Gross ML, Journal of the American Society for Mass Spectrometry, 2005, 16, 2057–2063. [PubMed: 16263307]
15. Monroe EB and Heien ML, Analytical chemistry, 2013, 85, 6185–6189. [PubMed: 23777226]
16. Cohn CA, Mueller S, Wimmer E and Schoonen M, Abstr Pap Am Chem S, 2004, 228, U698–U698.
17. Jones CD, Schlatterer JC, Brenowitz M and Pollack L, Lab on a chip, 2011, 11, 3458–3464. [PubMed: 21863183]
18. Schlatterer JC, Wieder MS, Jones CD, Pollack L and Brenowitz M, Biochemical and biophysical research communications, 2012, 425, 374–378. [PubMed: 22842460]
19. Puthussery J, Seefeld S, Berry N, Gibbs M and Law M, Journal of the American Chemical Society, 2011, 133, 716–719. [PubMed: 21175173]
20. Nguyen D, Taylor D, Qian K, Norouzi N, Rasmussen J, Botzet S, Lehmann M, Halverson K and Khine M, Lab on a chip, 2010, 10, 1623–1626. [PubMed: 20517559]
21. Nguyen D, McLane J, Lew V, Pegan J and Khine M, Biomicrofluidics, 2011, 5, 22209. [PubMed: 21799715]
22. Xu G, Kiselar J, He Q and Chance MR, Analytical chemistry, 2005, 77, 3029–3037. [PubMed: 15889890]
23. Nawarathna D, Norouzi N, McLane J, Sharma H, Sharac N, Grant T, Chen A, Strayer S, Ragan R and Khine M, Appl Phys Lett, 2013, 102, 63504. [PubMed: 23479497]

24. Pegan JD, Ho AY, Bachman M and Khine M, Lab on a chip, 2013, 13, 4205–4209. [PubMed: 24056907]
25. Lipinski B, Oxidative medicine and cellular longevity, 2011, 2011, 809696. [PubMed: 21904647]
26. Brenowitz M, Senear DF, Shea MA and Ackers GK, Methods in enzymology, 1986, 130, 132–181. [PubMed: 3773731]

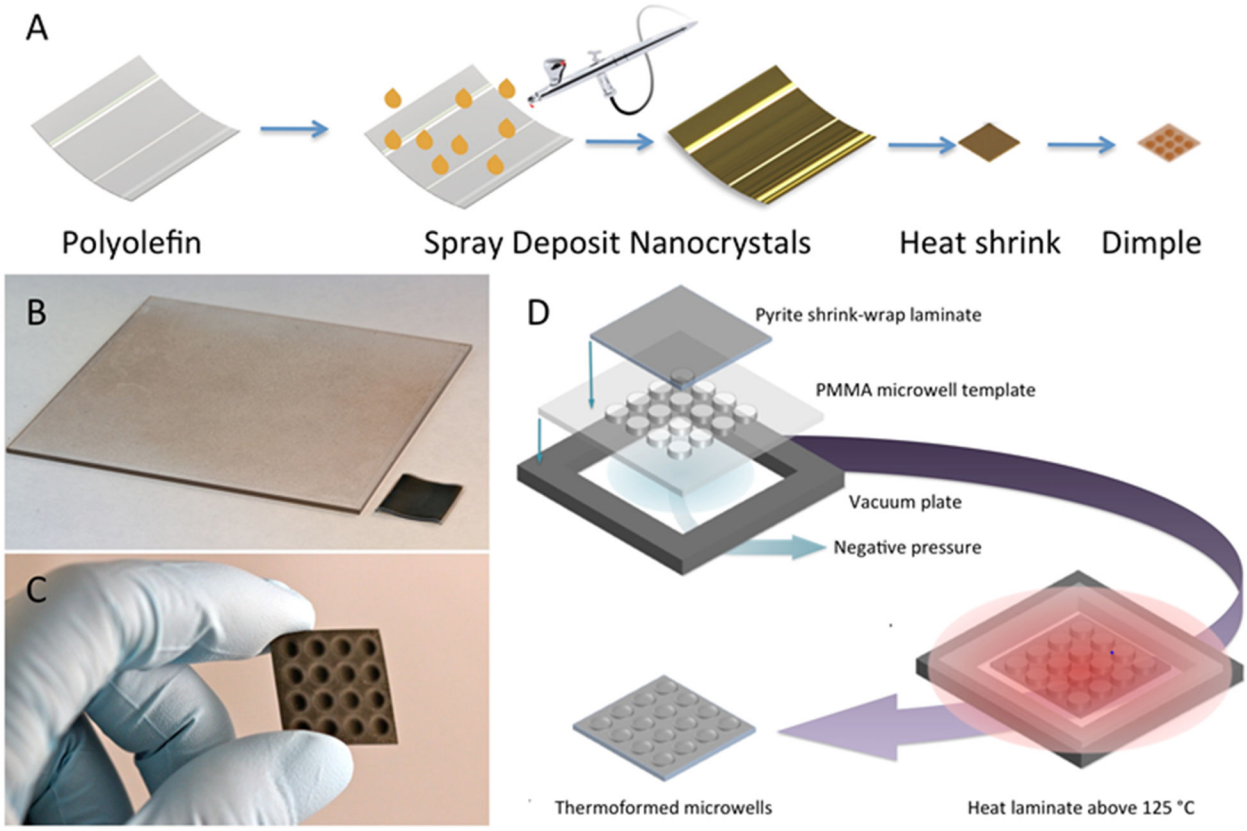

Fig. 1.

Fabrication of pyrite shrink-wrap laminate **(A)** The fabrication process. **(B)** Photographs of a substrate before (left) and after (right) thermal shrinking. **(C)** Image of a substrate complete with microwells. **(D)** Cartoon of the process for thermoforming the laminate to form microwells.

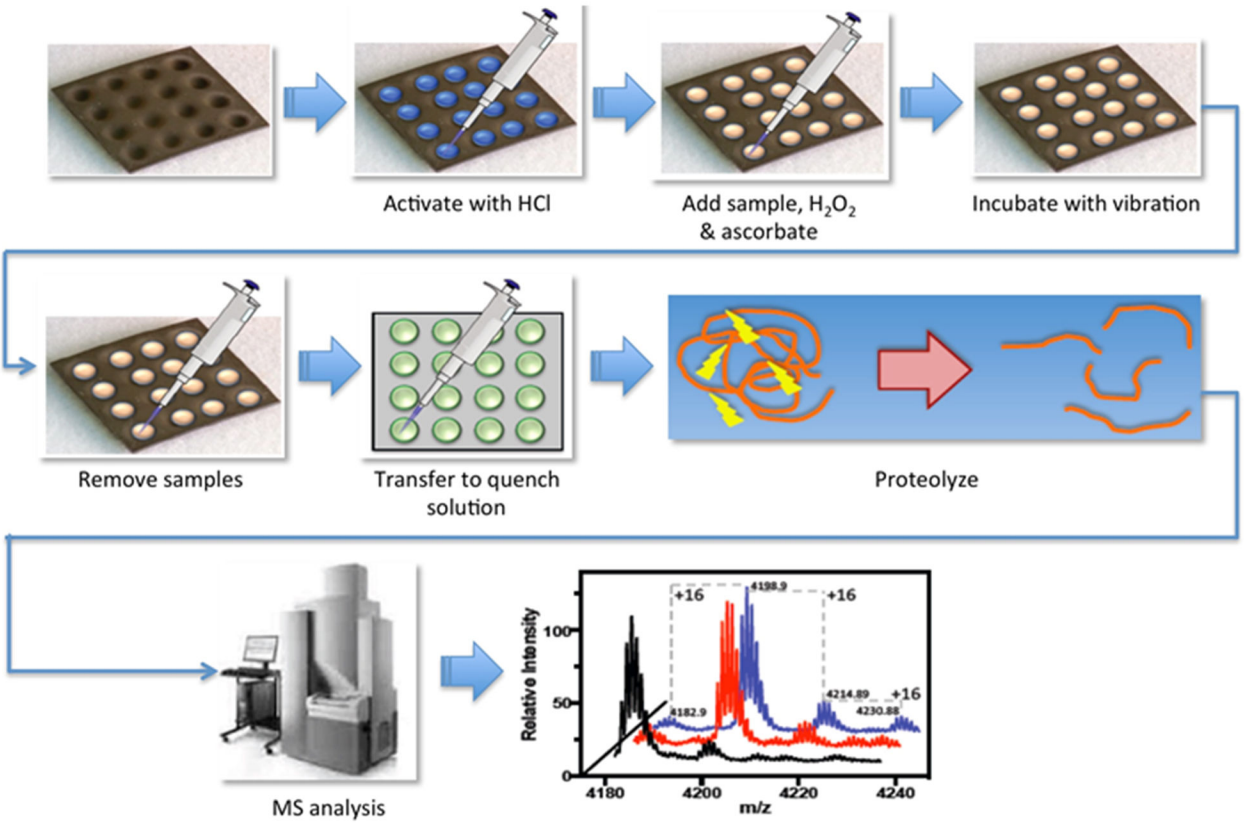

Fig 2.

Process flow summary for "drop deposition oxidative footprinting": *i*) surface oxidation is removed by acid wash followed by pH neutralization with multiple water washes; *ii*) H_2O_2 and ascorbate are added to a protein sample in standard reaction buffer to the desired concentrations; *iii*) 3 μL of the reaction mixture is pipetted into microwell and incubated with vibration for a defined period of time; *iv*) The sample is transferred to 27 μL of the quench solution; *v*) aliquots are removed from the quenched sample for proteolytic fragmentation and mass spectral analysis. Multiple samples can be processed in parallel using manual or robotic multichannel pipettes (not illustrated).

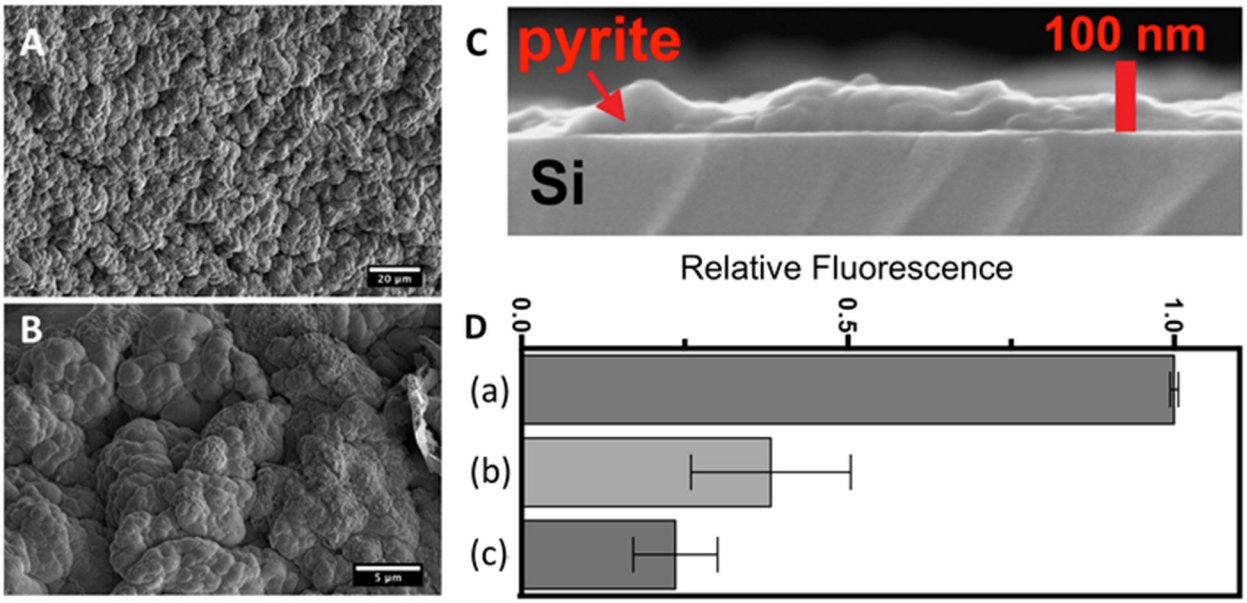

Fig 3.

(A & B) Top down SEMs showing the high-surface-area pyrite microstructure of laminate at medium and higher magnification; **(C)** SEM of the cross section of a pyrite nanocrystal film airbrushed onto silicon in a single pass. The silicon substrate facilitates the fracturing necessary for cross sectional imaging; **(D)** Solution drops of 3 μL containing fluorescent dye, 2 mM ascorbate and 8 mM H_2O_2 were incubated for 1 min in a microfuge tube (a), in a pyrite shrink-wrap microwell (b) and a microwell with vibration (c).

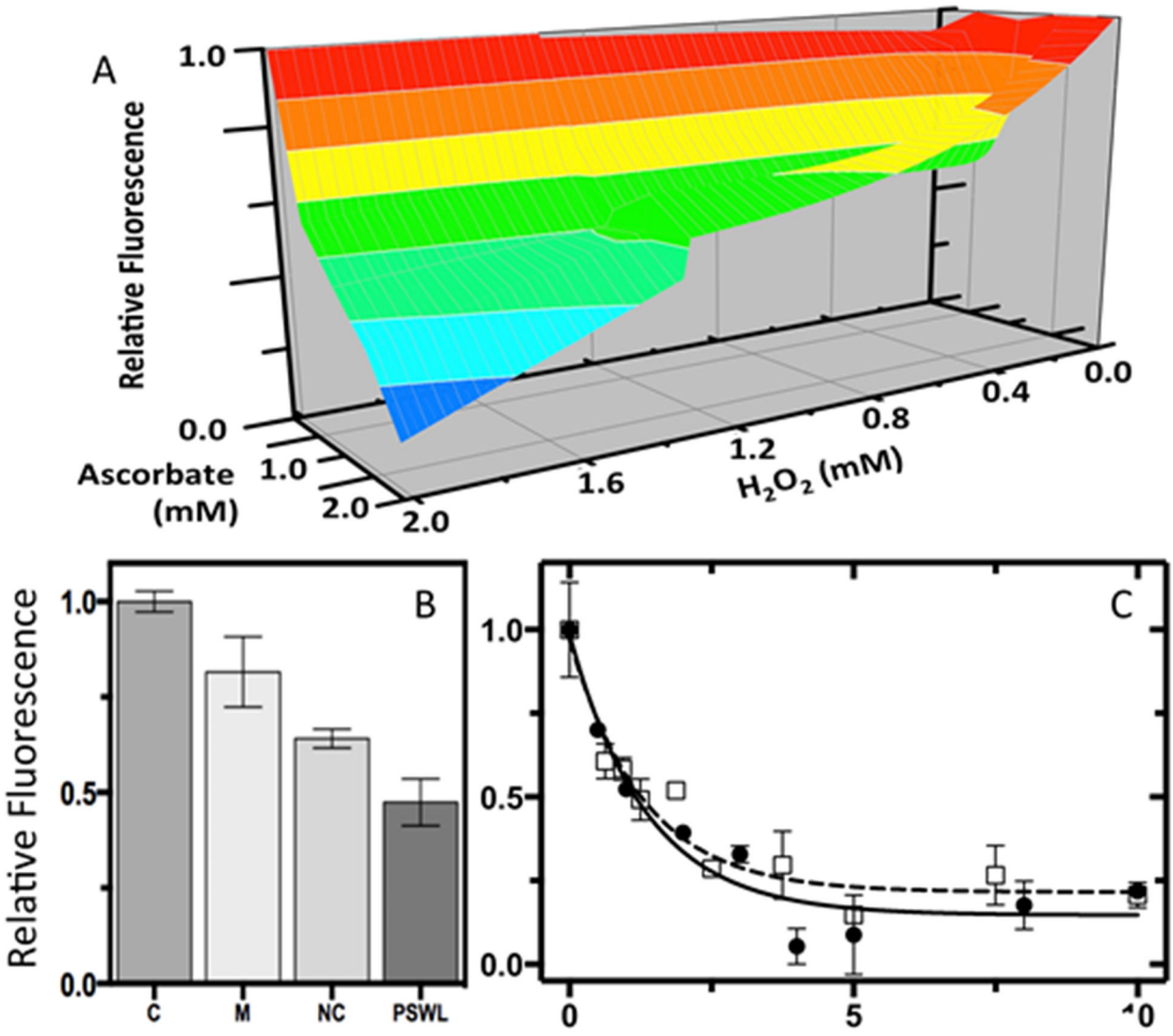

Figure 4:

Relative •OH production assayed by fluorescent dye degradation (see Supplement). ***(A)*** Quantitation of •OH production by pyrite shrink-wrap laminate as a function of H_2O_2 and ascorbate concentration at constant 5 min incubation; **(B)** Three μL buffered solution drops containing dye and 8 mM H_2O_2 and 2 mM ascorbate were incubated on a mineral pyrite surface, pyrite nanocrystals airbrushed onto a silicon wafer and pyrite shrink-wrap laminate with vibration. The control samples contained the same solutes but were not incubated on pyrite; **(C)** Dose-response curves relating •OH generation by pyrite shrink-wrap laminate at 2 mM ascorbate and 10 mM H_2O_2 as a function of incubation time in min (solid line) and at an incubation time of 5 min as a function of H_2O_2 concentration in mM (dashed line).

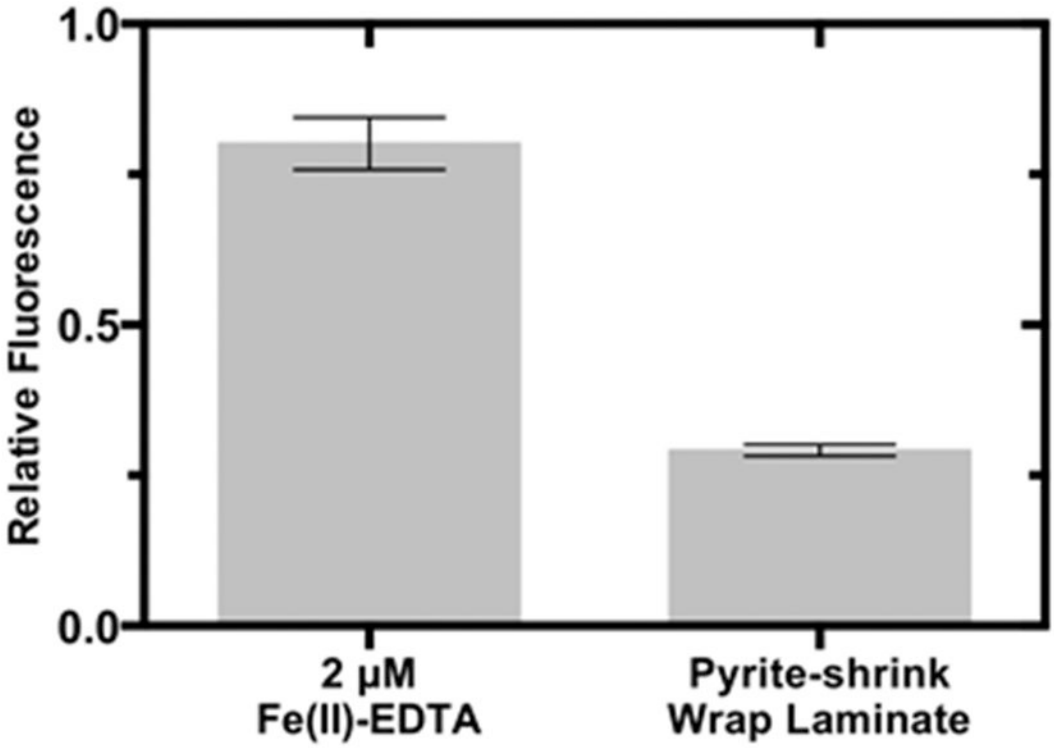

Figure 5:

Comparison of the relative oxidation by 2 μM Fe(II)-EDTA (roughly the amount of ferrous iron released into solution from pyrite shrink-wrap laminate), and the laminate itself. Two mM ascorbate with 15 mM H_2O_2 was present in both reactions with a 1 min incubation. Relative production of •OH assayed by degradation of a fluorescent dye as described in the Supplement.

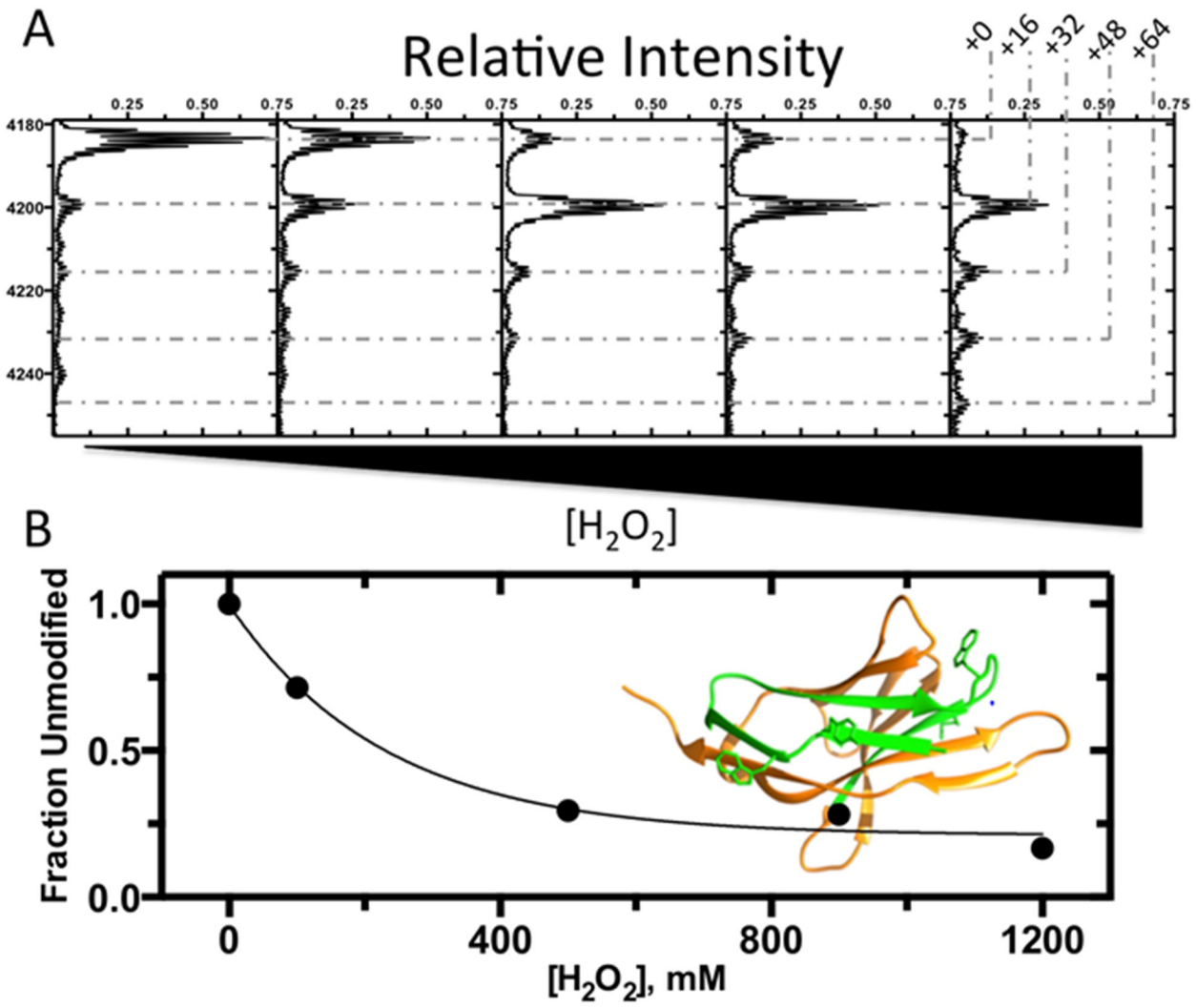

Figure 6:

Oxidation of the protein PD-1 by pyrite shrink laminate. Three μL of PD-1 in buffer containing 1 mM ascorbate and the indicated H_2O_2 concentration were incubated for 1 min with vibration on pyrite shrink-wrap laminate. Aliquots of the protein were proteolyzed and prepared for mass spectral analysis as described in *Experimental Design*. **A)** MALDI-MS1 analysis of the N-terminal tryptic peptide (residues 1-36) of PD-1 showing the multiples of +16 mass increases detected as a function of increasing concentrations of H_2O_2; **B)** The fraction of unmodified peptide as a function of H_2O_2 concentration. The solid line is an exponential fit to the data. *Insert:* Ribbon representation of the PD-1 structure highlighting the N-terminal peptide in green and the residues Y4, W8, W26, and M31 that are highly susceptible to oxidation.